J. Fluid Mech. (1978), *vol.* 88, *part* 4, *pp.* 711–735
Printed in Great Britain

Numerical study of the return of axisymmetric turbulence to isotropy

By U. SCHUMANN

Institut für Reaktorentwicklung, Kernforschungszentrum Karlsruhe,
7500 Karlsruhe, Postfach 3640, West Germany

AND G. S. PATTERSON

National Center for Atmospheric Research, Boulder, Colorado 80307

(Received 19 May 1975 and in revised form 8 January 1978)

The spectral method of Orszag & Patterson (1972*a*, *b*) is used here to study pressure and velocity fluctuations in axisymmetric, homogeneous, incompressible, decaying turbulence at Reynolds numbers $Re_\lambda \lesssim 40$. In real space 32^3 points are treated. The return to isotropy is simulated for several different sets of anisotropic Gaussian initial conditions. All contributions to the spectral energy balance for the different velocity components are shown as a function of time and wavenumber. The return to isotropy is effected by the pressure–strain correlation. The rate of return is larger at high than at low wavenumbers. The inertial energy transfer tends to create anisotropy at high wavenumbers. This explains the overrelaxation found by Herring (1974). The pressure and the inertial energy transfer are zero initially as the triple correlations are zero for the Gaussian initial values. The two transfer terms are independent of each other but vary with the same characteristic time scale. The pressure–strain correlation becomes small for extremely large anisotropies. This can be explained kinematically. Rotta's (1951) model is approximately valid if the anisotropy is small and if the time scale of the mean flow is much larger than $0{\cdot}2\,L_f/v$, which is the time scale of the triple correlations (L_f = integral length scale, v = root-mean-square velocity). The value of Rotta's constant is less dependent upon the Reynolds number if the pressure–strain correlation is scaled by v^3/L_f rather than by the dissipation. Lumley & Khajeh-Nouri's (1974) model can be used to account for the influence of large anisotropies. The effect of strain is studied by splitting the total flow field into large- and fine-scale motion. The empirical model of Naot, Shavit & Wolfshtein (1970) has been confirmed in this respect.

1. Introduction

The spectral method of Orszag & Patterson (1972*a*, *b*) has been used to simulate static-pressure and velocity fluctuations in incompressible homogeneous decaying turbulence. The method and its results for nearly isotropic turbulence have been presented in the companion paper (Schumann & Patterson 1978, hereafter referred to as I). The results have shown that the method is reliable for Reynolds numbers $Re_\lambda \leqslant 36$.†

† This is confirmed, moreover, by a comparison with the direct-interaction approximation in a paper (Schumann & Herring 1976) which has been prepared and published since the first version of the present paper was prepared.

Our study is concerned with axisymmetric anisotropic cases, for which we investigate the return to isotropy effected by the pressure–strain correlation. The pressure–strain correlation controls both the relative and the absolute magnitude of the Reynolds stresses and is thus one of the most important terms to be approximated in Reynolds-stress models of turbulence (see, for example, Reynolds 1976; Hanjalić & Launder 1972; Daly 1974; Donaldson 1972; Lumley & Khajeh-Nouri 1974). The simplest and most common assumption for this correlation is Rotta's (1951) 'return-to-isotropy' model.

However, even for homogeneous turbulence, the validity of this model has been questioned (Schumann 1975) and the magnitude of the empirical constant c in it is very uncertain. Values between 0·5 (Daly 1974) and 8 (Lumley & Khajeh-Nouri 1974) have been used even in the more recent literature, mainly because of a gap in experimental data. Most models are justified indirectly by comparison of their predictions for the Reynolds stresses with experiments, a typical comparison being that of Champagne, Harris & Corrsin (1970). Except for some measurements in the atmospheric boundary layer by Elliot (1972), no *direct* experimental results for the pressure–strain correlation are known. Elliot's results exhibit large statistical uncertainties, moreover. Deardorff (1974) and Schumann (1975) studied the pressure–strain correlation in a planetary boundary layer and in channel flows, respectively, at high Reynolds numbers, using finite-difference simulations for the large-scale motions together with some models for the subgrid-scale motions. In these studies the influence of the boundaries, the mean strain and the anisotropy of the length scales have not been separated, and their significance with respect to Rotta's model is therefore questionable.

The most direct investigation of this model has been made recently by Herring (1974) for axisymmetric turbulence using the direct-interaction approximation. He studied two forms of Rotta's return-to-isotropy model, one using E/ϵ and the other $L_f/E^{\frac{1}{2}}$ (E = energy, ϵ = dissipation, L_f = integral length scale) as the characteristic time scale. He found that the constant appearing in the second form is less dependent upon the initial conditions. One of the most surprising results was his finding of some 'overrelaxation', in that after some time the deviation from isotropy at high wavenumbers becomes opposite to that at small wavenumbers; this was not explained physically. Herring deduced the pressure–strain correlation from a balance between the time derivative of the energy, the nonlinear energy transfer and the rate of dissipation of energy.

In the present paper we also study axisymmetric turbulence as defined by some appropriate initial conditions. However, since we have access to the pressure fluctuations themselves, we are able to compute the pressure–strain correlation directly. This allows us to evaluate the spectral distribution and provides more insight into what is going on, especially with respect to the 'overrelaxation'. In addition to Rotta's proposal, we study the influence of anisotropic length scales, although success is marginal in this respect. Moreover, we evaluate the three constants appearing in Lumley & Khajeh-Nouri's (1974) proposal. We find that only two of them can be assumed to be universal.

Because of its technical importance, it would be helpful to have a method which allows the study of the impact of mean shear on homogeneous turbulence. This is not possible with the present scheme. However, we get some information about the

influence of mean shear by splitting the flow field into large- and fine-scale motions and using the spectral pressure–strain correlation.

As we start from random initial conditions, statistical errors appear which can be overcome only by the very expensive generation of large ensembles. The Reynolds number is low, so that no inertial subrange (Batchelor 1959) exists. Moreover, we are unable to use the initial conditions used by Herring (1974) because the truncation errors they would cause would be too large. The resultant constant in Rotta's model from the present simulations, however, is only slightly different from the values found by Herring. The return to isotropy in homogeneous turbulence with anisotropy induced by magnetohydrodynamical forces has been studied by Schumann (1976).

2. Run specifications

We use exactly the same method as in I except for the initial conditions. The spectral code integrates the velocities $\hat{u}_i(\mathbf{k}, t)$ as a function of time t for discrete values of the wavenumber vector $\mathbf{k} = \{k_1, k_2, k_3\} = k_{\min}\mathbf{N}$, where $\mathbf{N} = \{N_1, N_2, N_3\}$ are integer numbers with $|\mathbf{N}| < (242)^{\frac{1}{2}} \approx 15{\cdot}6$. The pressure in wavenumber space is $\hat{p}(\mathbf{k}, t)$. The Fourier transforms are the real-space variables $u_i(\mathbf{x}, t)$ and $p(\mathbf{x}, t)$, where $\mathbf{x} = \{x_1, x_2, x_3\}$. The computation involves 32^3 points in real space. Periodic boundary conditions are used ('box turbulence') with a periodic length $L = 2\pi/k_{\min}$.

The simplest anisotropic case is that of axisymmetric turbulence (Batchelor 1946). This case has been studied recently by Herring (1974). Using Herring's notation, axisymmetric turbulence (with zero helicity) can be described by

$$\langle \hat{u}_i(\mathbf{k}, t)\, \hat{u}_j(-\mathbf{k}, t)\rangle = \sum_{\alpha=1}^{2} \Phi^{\alpha}(\mathbf{k}, t)\, e_i^{\alpha}(\mathbf{k})\, e_j^{\alpha}(\mathbf{k}), \tag{1}$$

where the brackets denote the ensemble average,

$$\mathbf{e}^1(\mathbf{k}) = (\mathbf{k}\times\mathbf{n})/|\mathbf{k}\times\mathbf{n}|, \quad e^2(\mathbf{k}) = k\times\mathbf{e}^1(\mathbf{k})/|\mathbf{k}\times\mathbf{e}^1(\mathbf{k})| \tag{2}$$

and the Φ^{α} are two arbitrary scalar functions. The axis of symmetry is $\mathbf{n}$ and we choose

$$\mathbf{n} = (0, 0, 1). \tag{3}$$

Isotropic turbulence is recovered if $\Phi^1(\mathbf{k}, t) = \Phi^2(\mathbf{k}, t) = \hat{E}(\mathbf{k}, t)/(4\pi k^2)$, where $\hat{E}(k, t)$ is the energy spectrum. A method of generating Gaussian-distributed initial values for given values of $\Phi^{\alpha}(\mathbf{k})$ is described in the appendix. It is a generalization of the algorithm given by Orszag (1969) for isotropic initial fields. The general form of the prescribed values of $\Phi^{\alpha}(\mathbf{k})$ used here is

$$\Phi^{\alpha}(\mathbf{k}, 0) = \phi^{\alpha}(|\mathbf{k}|)\, \hat{E}(|\mathbf{k}|, 0)/(4\pi k^2) \quad (\alpha = 1, 2). \tag{4}$$

We consider four types of anisotropic initial fields (the details are given in table 1).

Type A.

$$\hat{E}(k, 0) = 16(2/\pi)^{\frac{1}{2}}\, v_0^2\, k_{\max}^{-5}\, k^2 \exp[-2(k/k_{\max})^2], \tag{5}$$

with

$$\phi^1(k) = 2, \quad \phi^2(k) = 0.$$

In this case $\hat{u}_3(\mathbf{k}, 0)$ is zero everywhere, whereas $\hat{u}_1(\mathbf{k}, 0)$ and $\hat{u}_2(\mathbf{k}, 0)$ have continuous non-zero spectra. This is not a two-dimensional initial state, since $\hat{u}_1(\mathbf{k}, 0)$ and $\hat{u}_2(\mathbf{k}, 0)$ depend on all three wavenumber components.

Run	$A1$	$A2$	$P1$	$P2$	$L1$	$L2$	$U1$	$U2$
Computer-job identifications	$F1, F2, F3$	$S2, S3, S4$	$D3$	$D4$	$K1$	$K2$	$U1$	$U2$
Wavenumber of energy peak, k_{max}	4·76	9·51	10	14	4·76	4·76	16	16
Scaling factor, k_{min}	2	2	2	2	2	2	2	2
R.m.s. velocity at time $t = 0$, v_0	1·014	0·994	0·823	0·832	1·06	1·11	1·01	1·29
Kinematic viscosity, ν	0·01189	0·0075	0·02	0·02	0·01189	0·01189	0	0
Maximum problem time, t_{max}	0·8	0·8	0·4	0·4	0·4	0·4	0·4	0·4
Time increment, Δt	0·008	0·01	0·01	0·01	0·01	0·01	0·01	0·01
Taylor microscale at time $t = 0$, λ_0	0·338	0·212	0·287	0·188	0·364	0·487	0·091	0·091
Integral length scale at $t = 0$, L_0	0·540	0·271	0·315	0·201	0·437	0·587	0·111	0·111

TABLE 1. Run specifications (runs $I1$–$I4$ are defined in I). All quantities are defined in arbitrary but consistent units.

Type P. $$\hat{E}(k,0) = \begin{cases} \frac{1}{2}k_{\min}^{-1} & \text{for} \quad k_{\max} - 2k_{\min} \leqslant |k| < k_{\max}, \\ 0 & \text{elsewhere,} \end{cases} \qquad (6)$$

$$\phi^1(k) = 2, \quad \phi^2(k) = 0.$$

In this case the velocities are zero initially except for $\hat{u}_1(\mathbf{k}, 0)$ and $\hat{u}_2(\mathbf{k}, 0)$, which are non-zero in a spherical shell in wavenumber space. This case is referred to as the 'peak case'.

Type L. In this case all velocities are non-zero and the energy spectrum is that given by (5). The initial field is constructed such that the mean-square values of all three velocity components are equal, but the length scales are different. These cases are used to test the hypothesis describing the influence of anisotropic length scales proposed by Schumann (1975). Here we use

$$\phi^2(|\mathbf{k}|) = 1 \text{ everywhere}$$

with $$\phi^1(|\mathbf{k}|) = \begin{cases} 0{\cdot}01 & \text{for} \quad |\mathbf{k}| \leqslant k_H \\ 3{\cdot}61 & \text{for} \quad |\mathbf{k}| > k_H \end{cases} \quad \text{for case } L1 \qquad (7a)$$

and $$\phi^1(|\mathbf{k}|) = \begin{cases} 3{\cdot}61 & \text{for} \quad |\mathbf{k}| \leqslant k_H \\ 0{\cdot}01 & \text{for} \quad |\mathbf{k}| > k_H \end{cases} \quad \text{for case } L2. \qquad (7b)$$

Here $k_H = 1{\cdot}04301\ k_{\max}$ is found from the condition

$$\int_0^{k_H} E(k,0)\,dk = \int_{k_H}^{\infty} E(k,0)\,dk.$$

Type U. Finally, we consider the case which has zero viscosity and is in equilibrium in $|\mathbf{k}|$ space but is initially anisotropic. The equilibrium spectrum for zero viscosity is (Lee 1952)

$$\hat{E}(k,0) = \tfrac{9}{2}v_0^2\, k_{\max}^{-3}\, k^2. \qquad (8)$$

We study two types of anisotropy:

$$\phi^1(k) = 2, \quad \phi^2(k) = 0 \quad \text{(case } U1\text{)},$$

$$\phi^1(k) = 0{\cdot}04, \quad \phi^2(k) = 3{\cdot}24 \quad \text{(case } U2\text{)}.$$

Two different cases of types A and P ($A1$, $A2$, and $P1$, $P2$) have been considered (the details are given in table 1). The results presented for runs $A1$ and $A2$ are the mean values taken over three independent realizations (ensemble means), each of which started from different random numbers with the same statistical properties. However, roughly 30 realizations would be needed in order to reduce statistical uncertainties below a desirable level for those statistics considered here.

No cases with energy spectra of the form ke^{-k} have been run because of the large truncation errors found for the corresponding isotropic case $I3$ in I. This, however, restricts the possibilities of direct comparison with Herring's (1974) results, for which this type of spectrum was used. However, direct comparisons showing good agreement are presented in Schumann & Herring (1976). The transition from a Gaussian initial state to a fully developed turbulent flow is discussed further in that paper.

3. Definition of statistics

We compute the dyadic product between the velocity vector $\mathbf{u}(\mathbf{k},t)$ and the components of the Navier–Stokes equation in wavenumber space (see I, for example),

$$\partial\hat{u}_i/\partial t - \nu k^2\hat{u}_i = \hat{\tau}_i \tag{9}$$

(ν is the kinematic viscosity and $\hat{\tau}_i(\mathbf{k},t)$ includes the inertial *and* pressure forces), and sume over shells around the origin in wavenumber space. This results in

$$\partial\hat{E}_{ij}/\partial t = \hat{\Gamma}_{ij} + \hat{\Phi}_{ij} - \hat{\epsilon}_{ij}. \tag{10}$$

This equation expresses the contributions of the inertia-transfer rate $\hat{\Gamma}_{ij}$, the pressure–strain rate $\hat{\Phi}_{ij}$, and the viscous dissipation rate $\hat{\epsilon}_{ij}$ to the variation of $\hat{E}_{ij}$, the tensorial energy spectrum. These terms and the pressure spectrum $\hat{P}$ are computed from

$$\left.\begin{matrix}\hat{E}_{ij}(k_0,t)\\ \hat{\epsilon}_{ij}(k_0,t)\\ \hat{\Upsilon}_{ij}(k_0,t)\\ \hat{\Phi}_{ij}(k_0,t)\\ \hat{P}(k_0,t)\end{matrix}\right\} = \sum_{k_0-\Delta k\leqslant|k|<k_0+\Delta k} \begin{cases} \hat{u}_i(\mathbf{k})\,\hat{u}_j(-\mathbf{k}), & (11a)\\ 2\nu k^2\hat{u}_i(\mathbf{k})\,\hat{u}_j(-\mathbf{k}), & (11b)\\ \hat{u}_i(\mathbf{k})\,\hat{\tau}_j(-\mathbf{k}) + \hat{u}_j(\mathbf{k})\,\hat{\tau}_i(-\mathbf{k}), & (11c)\\ -i(k_j\,\hat{u}_i(\mathbf{k}) + k_i\,\hat{u}_j(\mathbf{k}))\,\hat{p}(-\mathbf{k}), & (11d)\\ \hat{p}(\mathbf{k})\,\hat{p}(-\mathbf{k}). & (11e)\end{cases}$$

Here $\Delta k = \frac{1}{2}k_{\min}$. The transfer tensor $\hat{\Upsilon}_{ij}$ contains the contributions of both the inertial and the pressure forces. The strictly inertial energy transfer is found from

$$\hat{\Gamma}_{ij}(k,t) = \hat{\Upsilon}_{ij}(k,t) - \hat{\Phi}_{ij}(k,t). \tag{12}$$

If we contract the diagonal components, the pressure–strain contribution vanishes and we get the scalar equation

$$\partial\hat{E}/\partial t = \hat{\Upsilon} - \hat{\epsilon}, \tag{13}$$

where $$\hat{E}(k,t) = \tfrac{1}{2}\hat{E}_{ii}(k,t), \quad \hat{\epsilon}(k,t) = \tfrac{1}{2}\hat{\epsilon}_{ii}(k,t)$$

and $$\hat{\Upsilon}(k,t) = \tfrac{1}{2}\hat{\Upsilon}_{ii}(k,t) = \tfrac{1}{2}\hat{\Gamma}_{ii}(k,t).$$

We use the convention that repeated subscripts are summed from one to three. If we sum over all wavenumbers k, we get the real-space balances

$$\partial E_{ij}/\partial t = \Phi_{ij} - \epsilon_{ij}, \quad \partial E/\partial t = -\epsilon, \tag{14}$$

where $$E_{ij} \equiv \langle u_i u_j\rangle = \sum_k \hat{E}_{ij}(k), \quad E = \tfrac{1}{2}E_{ii},$$

$$\epsilon_{ij} \equiv 2\nu\left\langle \frac{\partial u_i}{\partial x_k}\frac{\partial u_j}{\partial x_k}\right\rangle = \sum_k \hat{\epsilon}_{ij}(k), \quad \epsilon = \tfrac{1}{2}\epsilon_{ii},$$

$$\Phi_{ij} \equiv \left\langle p\left(\frac{\partial u_i}{\partial x_j} + \frac{\partial u_j}{\partial x_i}\right)\right\rangle = \sum_k \hat{\Phi}_{ij}(k) = \sum_k \Upsilon_{ij}(k)$$

and $$\langle p^2\rangle = \sum_k \hat{P}(k).$$

We notice that Φ_{ij} can be calculated from $\hat{\Upsilon}_{ij}(k)$ without knowledge of the pressure field, since the net effect of the inertial energy transfer vanishes (Batchelor 1959,

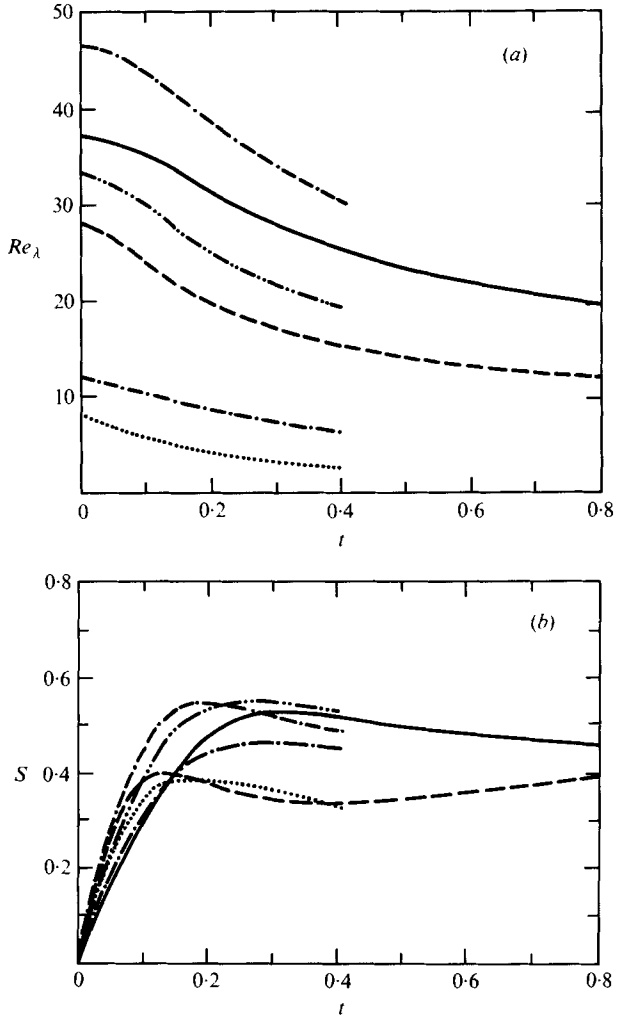

FIGURE 1. (*a*) Reynolds number and (*b*) skewness coefficient *vs.* time.
——, $A1$; — —, $A2$; —·—, $P1$; · · · · ·, $P2$; —··—, $L1$; - - -·- -, $L2$.

equation 5.2.14). This fact has been used to check the program. In addition, we evaluate tensorial integral length scales and the mean values of the pressure gradients:

$$L_{ij} = \frac{3}{4}\frac{\pi}{v^2}\sum_k \frac{1}{|\mathbf{k}|}\hat{u}_i(\mathbf{k})\,\hat{u}_j(-\mathbf{k}), \quad L_f = \tfrac{1}{3}L_{kk}, \tag{15}$$

$$\left\langle \frac{\partial p}{\partial x_i}\frac{\partial p}{\partial x_j}\right\rangle = \sum_k k_i k_j \hat{p}(\mathbf{k})\,(\hat{p}-\mathbf{k}), \tag{16}$$

$$v = (\tfrac{2}{3}E)^{\frac{1}{2}}. \tag{17}$$

We define, as usual, the Reynolds number $Re_\lambda = (v\lambda)/\nu$, where $\lambda^2 = 15\nu v^2/\epsilon$ is the Taylor microscale, and compute the skewness coefficient

$$S \equiv \tfrac{2}{35}[15\nu/\epsilon(t)]^{\frac{3}{2}}\sum_k k^2\hat{\Upsilon}(k),$$

which for isotropic turbulence is equal to $-\langle(\partial u_1/\partial x_1)^3\rangle/\langle(\partial u_1/\partial x_1)^2\rangle^{\frac{3}{2}}$ (Orszag & Patterson 1972*a*, *b*).

4. Time evolution of the anisotropic runs

The Reynolds number $Re_\lambda(t)$ and the skewness $S(t)$ are plotted *vs.* time in figures 1 (*a*) and (*b*). The decrease in the skewness for $0{\cdot}1 \leqslant t \leqslant 0{\cdot}4$ indicates some truncation errors for run $A2$, as described for the isotropic cases in I. At the cost of lower Reynolds numbers, truncation has been avoided in cases $P1$ and $P2$. The corresponding results for $U1$ and $U2$, which have infinite Reynolds numbers and zero skewness S, are not shown in these figures.

Typical plots of the time evolution are given in figure 2 for run $A2$, where the energy of the 3-component is zero initially. The return to isotropy can be clearly seen from the plots of E_{ij}, ϵ_{ij}, L_{ij} and $\langle(\partial p/\partial x_i)\,(\partial p/\partial x_j)\rangle$ *vs.* time t. For $i = j = 3$ we see a small increase during an initial phase ($t < 0{\cdot}05$); the increase then becomes steeper between $0{\cdot}05 \leqslant t \leqslant 0{\cdot}3$ and the viscous decay finally becomes dominant. We see that the return to isotropy is slow for L_{ij}, stronger for E_{ij} and strongest for ϵ_{ij} and the mean-square pressure gradients. (The mean-square value of the pressure gradient in the 3-direction is non-zero at time $t = 0$ because the velocities u_1 and u_2, and thus the pressure, are functions of x_3 at this time.) Thus the return to isotropy is strongest for those quantities which depend mainly upon the high wavenumber range. This return to isotropy is due to the pressure–strain correlation, which is also plotted in figure 2. We see that Φ_{11} and Φ_{22} are negative, whereas Φ_{33} is positive and the contraction is zero. These terms represent, therefore, the energy transfer from the 1- and 2-components to the 3-component. It is important to note that the Φ_{ij} are zero initially. Finally, figure 2 contains the normalized r.m.s. pressure fluctuation. This quantity is larger than one initially and decreases during the initial phase to settle between 0·9 and 1. Similar results were found for all the other runs (figure 3). For isotropic turbulence we found (I) values between 0·8 and 1·0 for all times. This is in contrast to the findings of Kraichnan (1956), who predicted that, for a given kinetic energy, isotropic turbulence produces higher pressure fluctuations than anisotropic turbulence.

Corresponding spectra at different times t are plotted in figures 4 and 5 (*a*) and (*b*). Figure 4 shows results which are very similar to those described for isotropic turbulence in I. Figures 5 (*a*) and (*b*) show the departure from isotropy $\Delta\hat{E}_{33}(k,t)$, where

$$\Delta\hat{E}_{ij}(k,t) = -[\hat{E}_{ij}(k,t) - \tfrac{1}{3}\delta_{ij}E_{kk}(k,t)], \tag{18}$$

the pressure–strain correlations $\hat{\Phi}_{ij}$ and the energy transfer $\hat{\Gamma}_{ij}$ by the inertial terms for two runs. Of special interest is figure 5 (*a*), which shows the results for run $P2$. As for the pressure in figure 4, we see that the pressure–strain correlation is distributed over a much broader wavenumber band than is the energy. This difference is explained by the fact that the pressure at some wavenumber $\mathbf{k}$ is a consequence of the interaction of velocities at $\mathbf{k}'$ and $\mathbf{k}''$, where $\mathbf{k} = \mathbf{k}' + \mathbf{k}''$. Also, the maximum pressure–strain rate occurs at higher wavenumbers than the maximum departure from isotropy; and the inertial transfer rates $\hat{\Gamma}_{ij}$ are just as anisotropic as the energy components $\hat{E}_{ij}$ in the sense that $|\hat{\Gamma}_{ij}|$ is proportional to $|\hat{E}_{ij}|$. It follows that the inertial transfer tends to create anisotropy at wavenumbers that are somewhat higher than the wavenumber at which the initial anisotropy dominates.

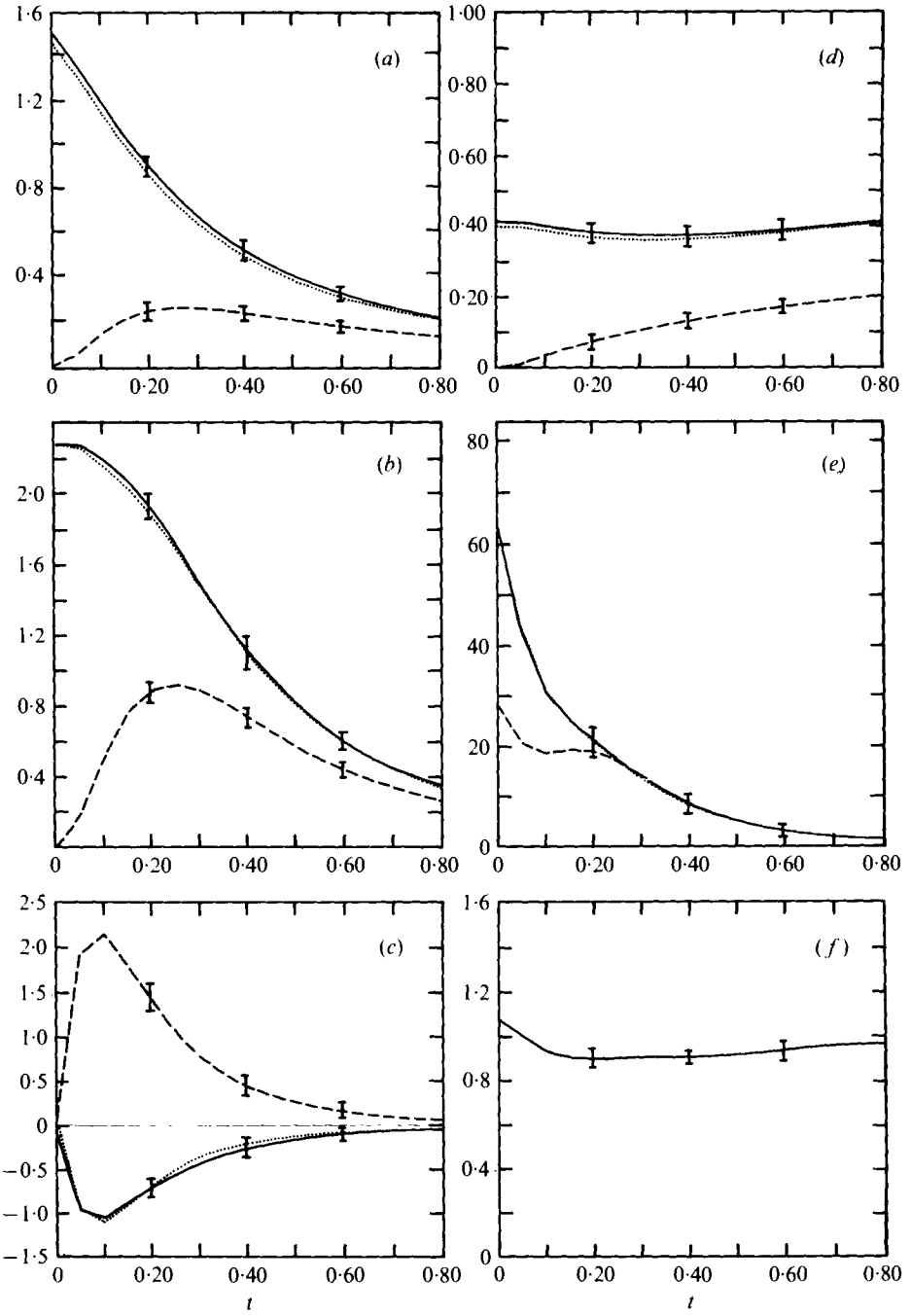

FIGURE 2. (*a*) Kinetic energy E_{ij}, (*b*) dissipation ϵ_{ij} and (*c*) pressure–strain correlation Φ_{ij} *vs.* time. (*d*) Length-scale tensor, L_{ij}, (*e*) mean-square pressure gradient $\langle(\partial p/\partial x_i)(\partial p/\partial x_j)\rangle$ and (*f*) r.m.s. pressure fluctuation $\langle p^2\rangle^{\frac{1}{2}}/v^2$ (normalized by the mean-square velocity) *vs.* time for run *A*2. ——, $(i,j) = (1,1)$; · · · · ·, $(i,j) = (2,2)$; — —, $(i,j) = (3,3)$.

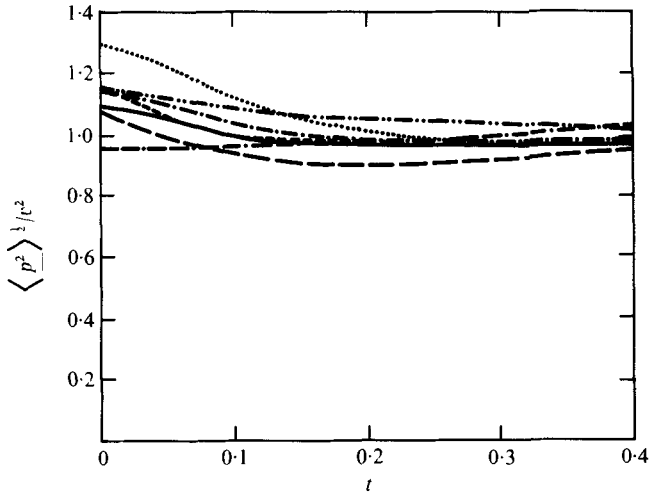

FIGURE 3. Normalized r.m.s. pressure fluctuations *vs.* time. ——, *A*1; — — —, *A*2; —·—, *P*1; · · · · ·, *P*2; —·—·—, *L*1; - - -·- - -, *L*2; – – – –, *U*1.

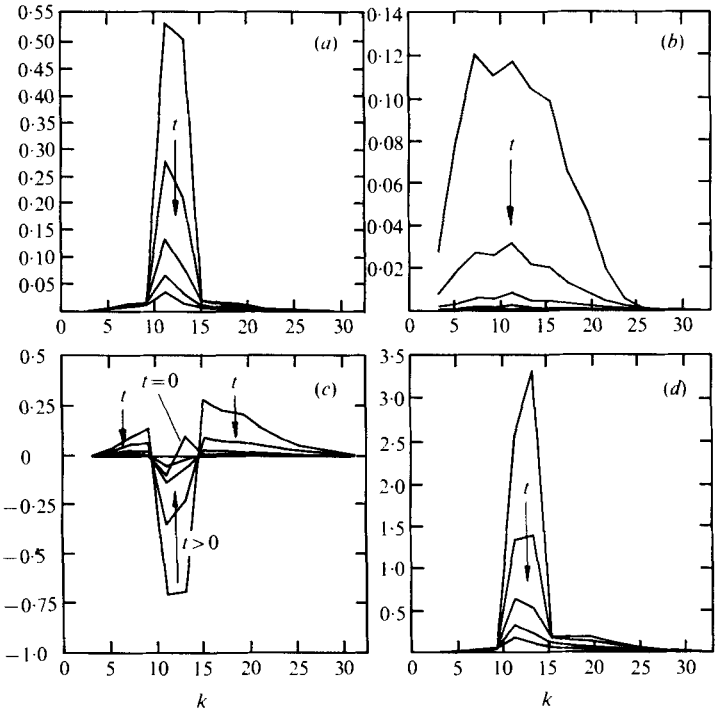

FIGURE 4. Spectral distribution of (*a*) the kinetic energy $\hat{E}(k,t)$, (*b*) the pressure $\hat{p}(k,t)$, (*c*) the transfer rate $\hat{\Upsilon}(k,t)$ and (*d*) the dissipation $\hat{\varepsilon}(k,t)$ *vs.* wavenumber for run *P*2 at times $t = 0, 0{\cdot}1, 0{\cdot}2, 0{\cdot}3$ and $0{\cdot}4$. Arrows indicate increasing time.

The ratios $r_{31}(k,t) \equiv \hat{E}_{33}(k,t)/\hat{E}_{11}(k,t)$ and $r_{21}(k,t) = \hat{E}_{22}(k,t)/\hat{E}_{11}(k,t)$ between the energies of different velocity components are illustrated in figures 6 and 7 (*a*)–(*c*). The degree of departure from axisymmetry due to statistical errors is seen from the ratio r_{21} in figure 7. The return to isotropy can be seen from r_{31}. We see that r_{31} generally

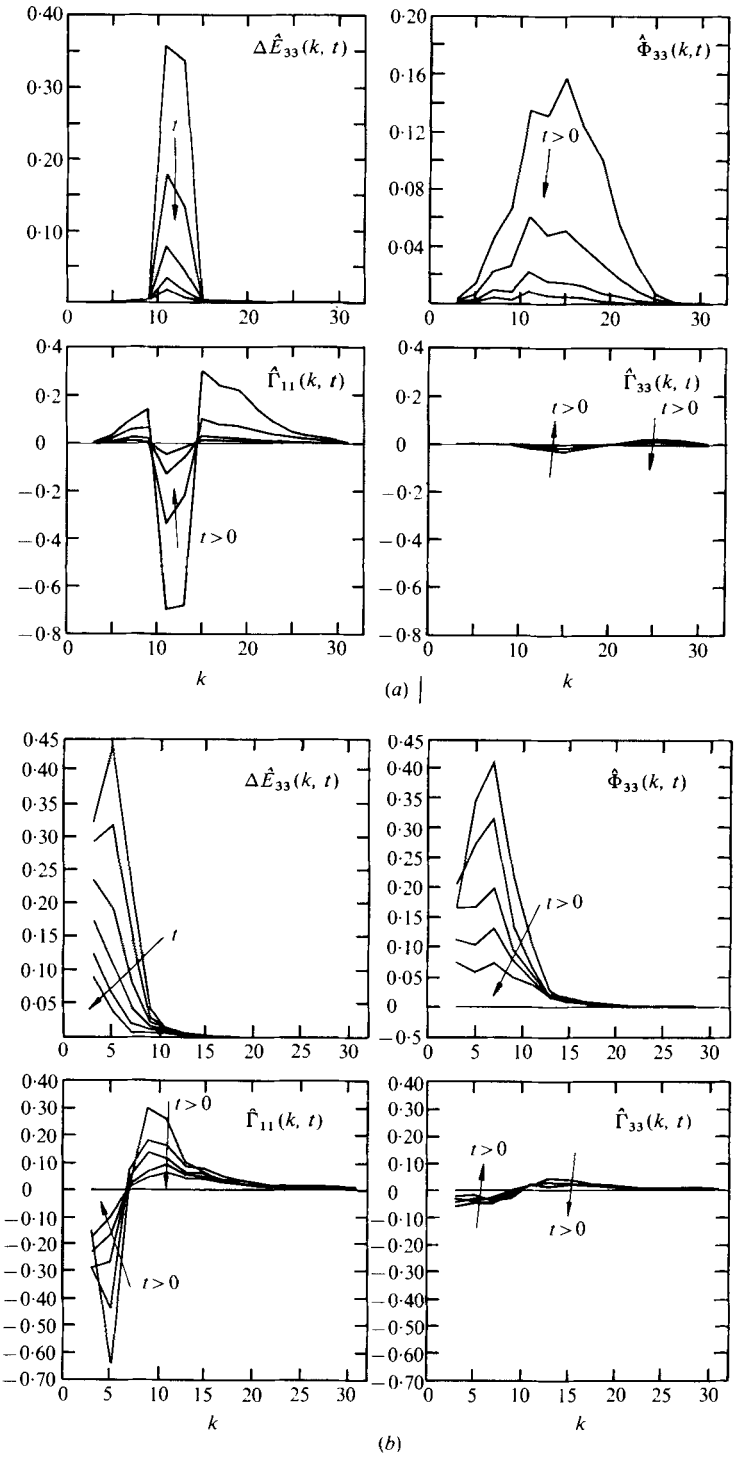

FIGURE 5. Departure from isotropy of the kinetic energy tensor, pressure transfer, and inertial transfer for the 1 and 3 components as a function of wavenumber k at times (*a*) $t = 0$, 0·1, 0·2, 0·3 and 0·4 for run *P*2 and (*b*) times $t = 0$, 0·16, 0·32, 0·48, 0·64 and 0·80 for run *A*1. Arrows indicate increasing time.

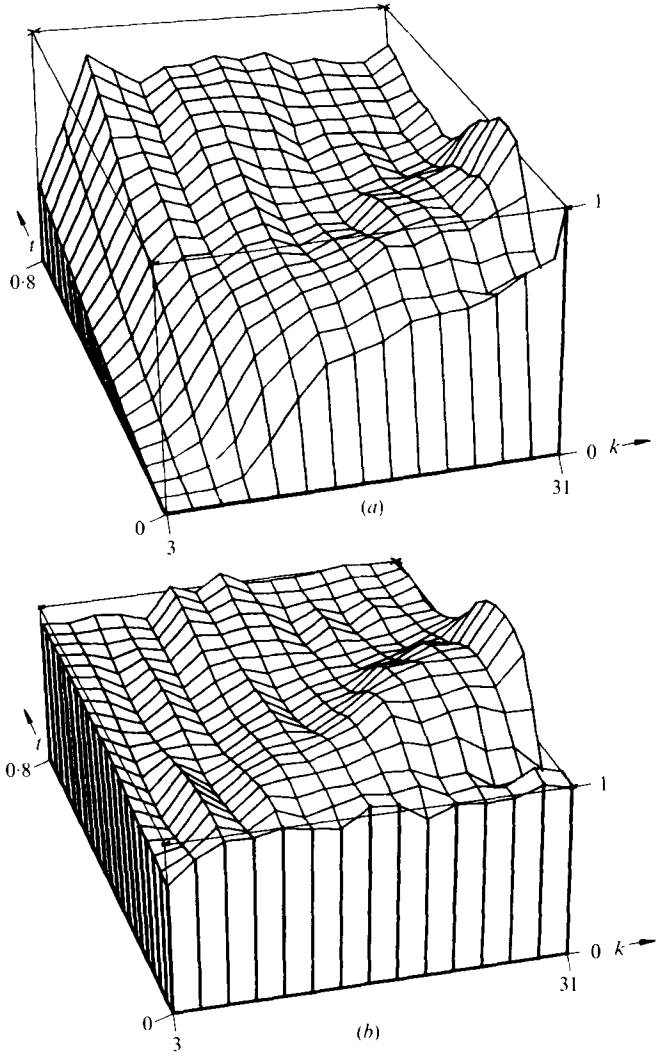

FIGURE 6. Energy ratios *vs.* wavenumber ($k = K$) and time ($t = T$) for run *A*1. The crosses denote unity. $3 \leqslant k \leqslant 31$, $0 \leqslant t \leqslant 0{\cdot}8$. (*a*) $\hat{E}_{33}/\hat{E}_{11}$. (*b*) $\hat{E}_{22}/\hat{E}_{11}$.

tends to approach the 'isotropic' value one and that this tendency is, at least initially, stronger at higher wavenumbers than at lower ones. This tendency shows the effect of the inertial and pressure transfer terms only; it is not influenced by the viscous dissipation directly. This can be seen from

$$\frac{\partial r_{31}}{\partial t} = \frac{\hat{E}_{11}\,\partial \hat{E}_{33}/\partial t - \hat{E}_{33}\,\partial \hat{E}_{11}/\partial t}{\hat{E}_{11}^2}. \tag{19}$$

Since the contribution to $\partial \hat{E}_{ij}/\partial t$ produced by the dissipation is $\nu k^2 \hat{E}_{ij}$, there is no variation of r_{31}. In other words, the ratio between the energy components would not change if there were viscous dissipation only.

However, some tendency away from the isotropic state can be seen for cases *P*1 and *P*2 in figure 7 (*b*). Here we see that r_{31} approaches the value one only in the region

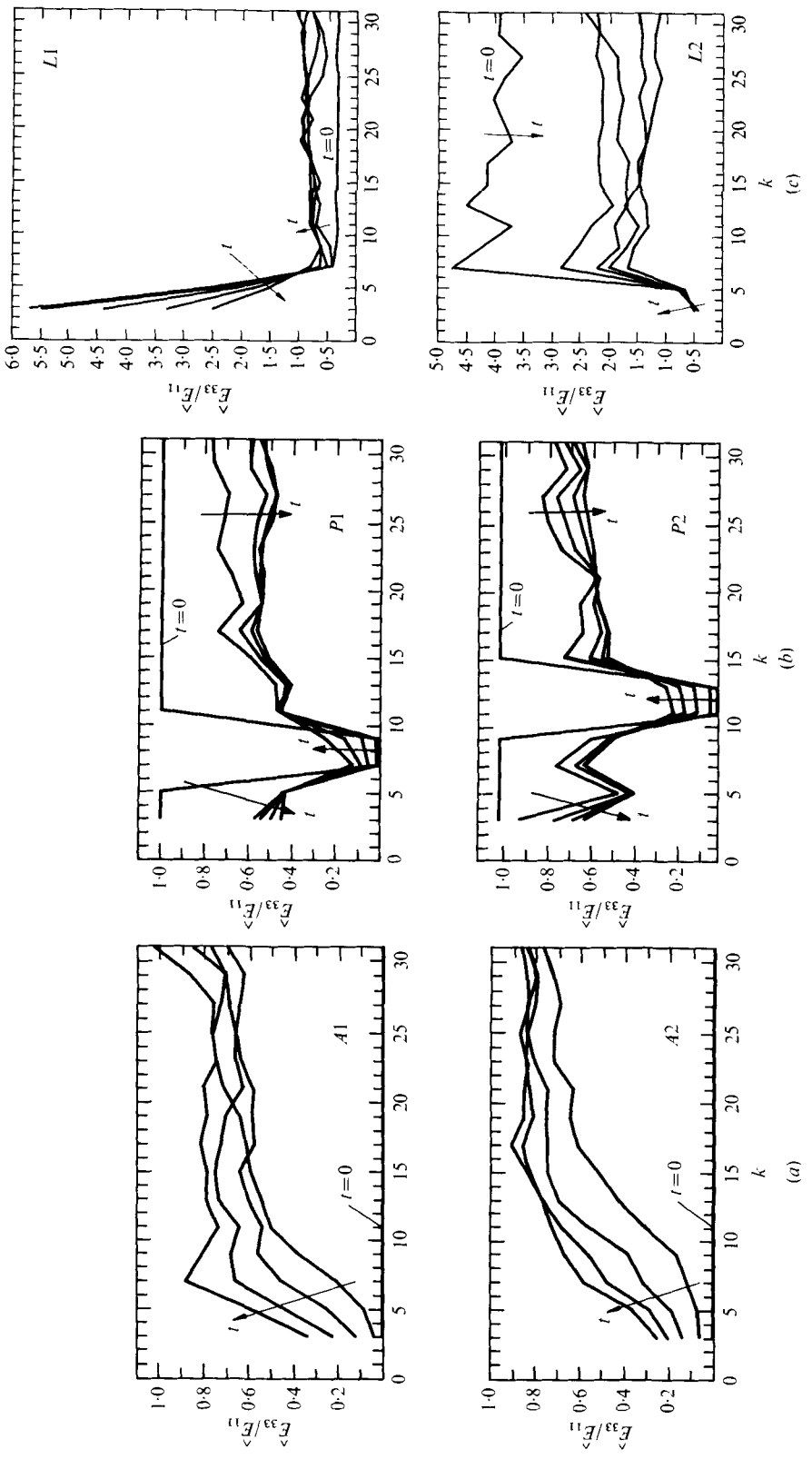

FIGURE 7. Energy ratios *vs.* wavenumber k at (*a*) times $t = 0$, 0·2, 0·4, 0·6 and 0·8 for runs *A*1 and *A*2, (*b*) times $t = 0$, 0·1, 0·2, 0·3 and 0·4 for runs *P*1 and *P*2 and (*c*) times $t = 0$, 0·1, 0·2, 0·3 and 0·4 for runs *L*1 and *L*2. Arrows indicate increasing time.

of the initial energy peak. Outside this region, r_{31} tends to deviate from the isotropic state, especially for the first time steps. Later on, the variation of r_{31} becomes smaller and we expect that it will return to one after some time. This effect can be explained as due to the anisotropy in the inertial energy transfer $\hat{\Gamma}_{ij}(k, t)$, which creates anisotropy in those regions where the energy is much smaller than in the peak region. If we substitute (10) into (19) and assume $\hat{E}_{11}(k) \approx \hat{E}_{33}(k)$ for this high wavenumber region, we get

$$\partial r_{31}/\partial t \approx (\hat{\Gamma}_{33} + \hat{\Phi}_{33} - \hat{\Gamma}_{11} - \hat{\Phi}_{11})/\hat{E}_{11}.$$

From $\hat{\Phi}_{ii} = 0$ and $\hat{\Phi}_{11} = \hat{\Phi}_{22}$ it follows that

$$\partial r_{31}/\partial t \approx (\hat{\Gamma}_{33} + \tfrac{3}{2}\hat{\Phi}_{33} - \hat{\Gamma}_{11})/\hat{E}_{11}. \tag{20}$$

Here all quantities are positive. If $\hat{\Gamma}_{33} \simeq 0$, we see that r_{31} decreases if $\hat{\Gamma}_{11} > \frac{3}{2}\hat{\Phi}_{33}$ and this is true for cases $P1$ and $P2$ at high wavenumbers (see figure 5*a*).

On the other hand, Herring (1974) found just the opposite effect in his simulations using the direct-interaction approximation: with $r_{31} < 1$ everywhere initially, he found that r_{31} became larger than one at high wavenumbers and remained smaller than one at low wavenumbers.† The important difference between Herring's simulation and the present one lies in the fact that his initial spectrum is proportional to e^{-k} and thus decreases much more slowly than the spectra considered here. In this case, $\hat{\Gamma}_{33}$ is not zero and the pressure–strain correlation is larger, so that $\frac{3}{2}\hat{\Phi}_{33} + \hat{\Gamma}_{33}$ becomes larger than $\hat{\Gamma}_{11}$ at high wavenumbers. In this case, it follows from (20) that r_{31} increases, which explains the overrelaxation at large wavenumbers. However, in both cases the energy content at high wavenumbers is small, so that in the overall behaviour (E_{33}/E_{11}) such an overrelaxation does not appear.

We saw that the pressure–strain correlation tends to be large at wavenumbers that are larger than those where the maximum anisotropy exists. To quantify this finding, we calculate the correlation coefficient

$$K(\gamma) = \frac{\Sigma \dfrac{\hat{\epsilon}(p,t)}{\hat{E}(p,t)} \Delta\hat{E}_{ij}(p,t)\,\hat{\Phi}_{ij}(k,t)}{\left[\left(\Sigma \left(\dfrac{\hat{\epsilon}(p,t)}{\hat{E}(p,t)} \Delta\hat{E}_{ij}(p,t)\right)^2\right)(\Sigma\hat{\Phi}_{ij}^2(k,t))\right]^{\frac{1}{2}}} \qquad (p = \gamma k) \tag{21}$$

and determine the value $\gamma_{\max}$ of the factor γ for which $K(\gamma)$ takes its maximum value. $\gamma_{\max}$ is then a measure of the ratio of the wavenumbers at which the pressure–strain correlation is significant to those at which the anisotropy is dominant. From (11) it follows that $\gamma_{\max} = 1$ if the velocity field is non-zero only in a thin shell in wavenumber space. Otherwise, $\gamma_{\max}$ is less than 1. From the simulations we find $\gamma_{\max} = 0{\cdot}7 \pm 0{\cdot}2$, which indicates that the pressure–strain correlation at some wavenumber is the result of the anisotropy at a wavenumber that is smaller by about a factor of 0·7.

Finally, it should be noted that the return to isotropy exists even in the inviscid equilibrium cases $U1$ and $U2$; this can be seen for run $U2$ from figure 8. Here, again, Φ_{33} is zero initially.

† Actually, Herring plotted the ratio $R \equiv E_2/E_1 = \Phi^2/\Phi^1$. From equation (A 2) in the appendix (assuming Φ^1 and Φ^2 to be functions of $|\mathbf{k}|$ only) it follows that $r_{31} \hat{=} 4R/(3+R)$. This means that $r_{31} = 1$ if $R = 1$ and the departure from one is of the same sign as $(1-r_{31})\,(1-R) \geqslant 0$. (The assumption of angular invariance of $\Phi^\alpha(\mathbf{k})$ has been made by Herring for most of his runs.)

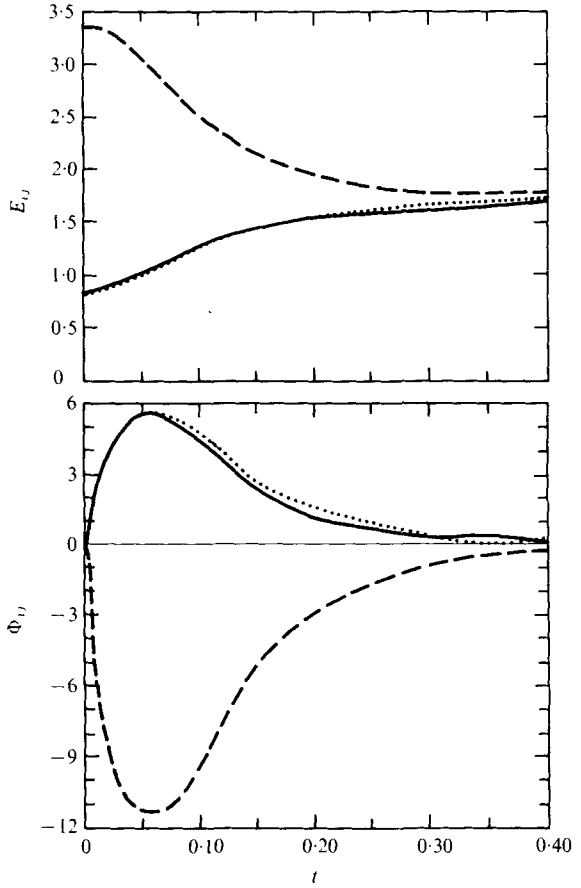

FIGURE 8. Kinetic energy E_{ij} and pressure–strain correlation Φ_{ij} *vs.* time t for run $U2$. ——, $(i,j) = (1,1)$; · · · · · ·, $(i,j) = (2,2)$; — —, $(i,j) = (3,3)$.

There are two reasons why the pressure–strain correlation is zero initially. First, the initial velocity field is Gaussian and triple velocity correlations are consequently zero. The pressure–strain correlation can be expressed as a function of the velocity field (using, for example, Uberoi's (1953) theory):

$$\Phi_{ij}(\mathbf{x}) = \frac{1}{4\pi}\int_V \frac{\partial^2}{\partial y_m \partial y_n}\left\langle u_m(\mathbf{x})\, u_n(\mathbf{x})\left(\frac{\partial u_i(\mathbf{y})}{\partial x_j}+\frac{\partial u_j(\mathbf{y})}{\partial x_i}\right)\right\rangle \frac{dV(\mathbf{y})}{|\mathbf{y}-\mathbf{x}|}. \tag{22}$$

We see that Φ_{ij} is zero if the triple correlations are zero. Non-zero triple correlations are produced by the dynamics of the flow. Those triple correlations which determine Φ_{ij} are different, however, from those describing the inertial energy transfer from small to large wavenumbers. For axisymmetric turbulence the triple correlations can be expressed as a function of five independent scalar functions (Batchelor 1946). Only one of them determines the skewness coefficient S. The skewness is zero for cases $U1$ and $U2$, and this shows the independence of the inertial energy transfer to larger wavenumbers from the energy transfer between the different velocity components at fixed scalar wavenumbers. The second reason for zero initial values of Φ_{ij} is kinematic in nature. The correlation Φ_{ii} is zero by definition if $\partial u_i/\partial x_j + \partial u_j/\partial x_i$ is zero everywhere. In most runs we start with $u_3 \equiv 0$ and therefore $\partial u_3/\partial x_3 = 0$, which results in

zero Φ_{33} values. Because of symmetry and continuity we also have $\Phi_{11} = \Phi_{22} = 0$. This shows that we have to expect a decrease in the pressure–strain correlations for very strong anisotropies for kinematical reasons.

5. Discussion of empirical models for the pressure–strain correlation

5.1. *Rotta's model*

Rotta (1951) proposed a simple relationship between the pressure–strain correlation Φ_{ij} and the departure from isotropy ΔE_{ij} which can be expressed in one of the two following forms (also considered by Herring 1974):

$$\Phi_{ij} \approx c \frac{\epsilon}{E} \Delta E_{ij} \tag{23}$$

or

$$\Phi_{ij} \approx c' \frac{E^{\frac{1}{2}}}{L_f} \Delta E_{ij}, \tag{24}$$

where L_f is defined by (15), $\quad \Delta E_{ij} = -(E_{ij} - \frac{1}{3}\delta_{ij} E_{kk}),$ (25)

and c and c' are expected to be positive constants of order unity. These forms are equivalent if $\epsilon = (c' E^{\frac{3}{2}})/(c L_f)$, which is true only in the limit of very high Reynolds number and for steady flows (see I). The Rotta model assumes that the pressure–strain correlation is kinematically determined by the departure from isotropy (see Rotta 1951, figure 2). We have shown above, however, that this is not true. On the other hand, Rotta's model does not account for the kinematical constraint that $\Phi_{ij} = 0$ if $\partial u_i/\partial x_j + \partial u_j/\partial x_i = 0$. Rotta's model is therefore valid only if the flow is steady and if the departures from isotropy are small.

We determine c and c' (which are called 'constants' and assumed to be independent of i and j) by a least-squares fit, so that

$$\sum_{i=1}^{3} \sum_{j=1}^{3} [\Phi_{ij}(t) - \Phi_{ij}^m(t)]^2 = \text{minimum}. \tag{26}$$

Here Φ_{ij}^m is the value given by the right-hand side of either (23) or (24). The resultant functions $c(t)$ and $c'(t)$ are plotted *vs.* time t for several runs in figure 9. The initial phase during which the triple correlations are built up is clearly reflected in the fact that $c(t)$ and $c'(t)$ are zero initially and grow rapidly to some value of order unity. If we compare the time evolution of these 'constants' with the time evolution of the skewness $S(t)$ (figure 1*b*), we see that the times needed to establish the triple correlations for the energy transfer and the pressure–strain correlation, respectively, are about the same and of order $0{\cdot}2\, L_f/v$. This is especially evident for runs $A1$ and $A2$, which have different time scales.

Using (26) but summing in addition over all times $t > 0{\cdot}2\, L_f/v$, we get mean values for the constants c and c' that are characteristic of the complete run. These are listed in table 2 together with the resultant r.m.s. errors:

$$\left.\begin{matrix}\delta = \\ \delta' =\end{matrix}\right\} \{[\textstyle\sum (\Phi_{ij}(t) - \Phi_{ij}^m(t))^2]/[\sum \Phi_{ij}^2(t)]\}^{\frac{1}{2}}, \quad \begin{cases}\Phi_{ij}^m \text{ from (23)}, & (27a) \\ \Phi_{ij}^m \text{ from (24)}. & (27b)\end{cases}$$

We see that these errors are very large for the approximately isotropic runs $I1$–$I4$ described in I. In these cases the systematic departure from isotropy is small compared with statistical fluctuations. Moreover, the sign of the anisotropy might change

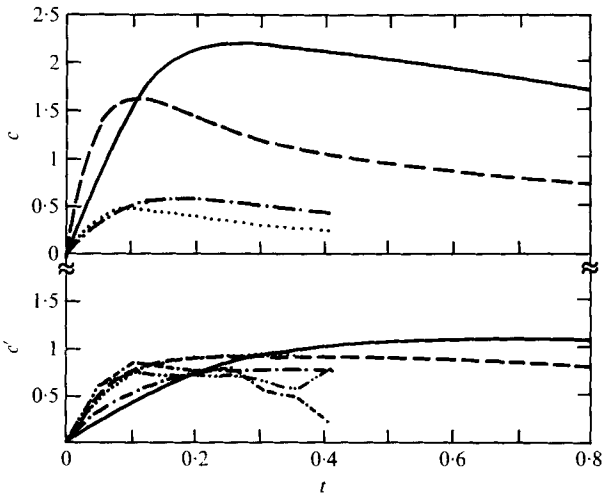

FIGURE 9. Rotta's constants c and c' *vs.* time. ——, $A1$; – – –, $A2$; —·—, $P1$; ·····, $P2$; —··—, $U1$; – –·– –, $U2$ ($c = \infty$ for $U1$ and $U2$).

Run	c	c'	δ	δ'
$I1$	0·038	−0·112	0·9998	0·995
$I2$	−0·157	−0·207	0·991	0·971
$I3$	−0·422	−0·539	0·919	0·921
$I4$	−0·395	−1·45	0·747	0·747
$A1a$	1·89	0·752	0·295	0·378
$A1b$	2·13	0·780	0·190	0·177
$A1c$	2·03	0·779	0·239	0·317
$A1$	2·06	0·787	0·148	0·237
$A2a$	1·48	0·837	0·143	0·095
$A2b$	1·37	0·761	0·211	0·163
$A2c$	1·35	0·782	0·144	0·067
$A2$	1·41	0·799	0·148	0·084
$P1$	0·536	0·545	0·178	0·223
$P2$	0·376	0·550	0·121	0·234
$L1$	1·34	0·613	0·770	0·800
$L2$	3·78	1·20	0·312	0·191
$U1$	∞	0·635	1·000	0·166
$U2$	∞	0·651	1·000	0·180

TABLE 2. Rotta's constants c and c' and r.m.s. errors δ and δ' (see § 5.1).

during the run. In order to balance this anisotropy, the triple correlations appearing in (22) must change their sign. This change takes some time, during which Φ_{ij} and ΔE_{ij} can have opposite signs, which explains the negative values we find for c and c' in these cases.

The errors are much smaller for the runs with large anisotropies. The smallest errors appear for runs $A1$ and $A2$. If these are compared with the results obtained for the three realizations (a, b, c) we see the importance of ensemble averaging. However, we find that the quadratic errors for the ensemble means are larger than one-ninth of the

sum of the quadratic errors for the single runs. This indicates that these errors are in fact composed of statistical fluctuations and systematic deviations. For these runs the systematic errors are smaller than 0·1. It is important to note that the values of the constants found for a single realization are not systematically different from those found for the ensemble mean values; we can therefore assume that the results will not change very much if we average over larger ensembles. Figure 9 and table 2 show that the value of c' is less dependent upon the initial values than the value of c. The characteristic time scale of the return to isotropy is therefore $L_f/E^{\frac{1}{2}}$ rather than E/ϵ; this is especially evident from runs $U1$ and $U2$, where $c = \infty$. This result was also obtained by Herring (1974). It is a reasonable finding, since the pressure–strain correlation is large in the energy-containing region, which does not contribute to the dissipation directly. We find a mean value $c' \approx 0{\cdot}7 \pm 0{\cdot}2$, which is about 20% smaller than the values found by Herring (1974). This difference may result from the restricted number of modes retained in Herring's model (discussed in Schumann & Herring 1976). For the other model the value of the factor c varies between 0·4 and 3·8.

5.2. *Effect of scale anisotropy*

Schumann (1975) has investigated high Reynolds number channel flows and calculated the pressure–strain correlation as well as the 'constant' c. He found different values for c depending on the subscripts i and j of Φ_{ij}. He gave some arguments that explained this result by the anisotropy in the length scales: if for any component of ΔE_{ij} and Φ_{ij} $(i = j)$ the corresponding value of L_{ij} is large, then the resultant value of c is small. In order to test this hypothesis we ran cases $L1$ and $L2$. Here the L_{ij} are strongly anisotropic. (At $t = 0$, we have $L_{11} = L_{22} = 0{\cdot}36$ and $L_{33} = 0{\cdot}59$ for $L1$ and $L_{11} = L_{22} = 0{\cdot}68$ and $L_{33} = 0{\cdot}42$ for $L2$; these values do change, but only by $\pm 0{\cdot}05$ during the run until $t = 0{\cdot}4$.) However, we cannot expect different values of c for different values of i and j since, in the axisymmetric case, we have $\Phi_{11} = \Phi_{22} = -\frac{1}{2}\Phi_{33}$ and $\Delta E_{11} = \Delta E_{22} = -\frac{1}{2}\Delta E_{33}$, which implies that c is independent of i and j $(i = j)$.

We have been unable to find any empirical correlation that satisfactorily describes the influence of the length-scale anisotropy. We experimented with

$$\Phi_{ij} = c' \frac{E^{\frac{1}{2}}}{L_f} \Delta E_{ij} + c'' \frac{E^{\frac{3}{2}}}{L_f^2} \Delta L_{ij} \tag{28}$$

and

$$\Phi_{ij} = c''' \frac{\{(\Delta E_{ij})^2 (\Delta L_{ij})^2\}^{\frac{1}{2}}}{\Delta E_{ij} \Delta L_{ij}} \frac{E^{\frac{1}{2}}}{L_f} \Delta E_{ij}, \tag{29}$$

where

$$\Delta L_{ij} = L_{ij} - \tfrac{1}{3}\delta_{ij} L_{kk}, \quad L_f = \tfrac{1}{3} L_{kk}.$$

The correlation coefficient between ΔE_{ij} and ΔL_{ij}, the reciprocal of which appears in the second proposal, is very near to one in all the runs considered here. It does not change the predicted value of Φ_{ij} appreciably if (29) is used. Also the values of c' and c'' are not independent in these cases. Many more different wavenumbers $\mathbf{k}$ must be included in the simulation in order to allow independent variation of ΔL_{ij} and ΔE_{ij}.

Run	*A*1	*A*2	*P*1	*P*2	*U*1	*U*2
c_1	1·24	0·977	1·08	1·44	0·761	0·848
c_2	−4·25	−2·00	−4·04	−6·41	−1·56	−2·45
δ	0·146	0·050	0·170	0·083	0·101	0·089

TABLE 3. Constants appearing in the model of Lumley & Khajeh-Nouri (1974); $c_3 \equiv 0$ (see § 5.3).

5.3. *Evaluation of the proposal of Lumley & Khajeh-Nouri*

Another proposal for refining Rotta's model based on purely formal arguments is that of Lumley & Khajeh-Nouri (1974):

$$\Phi_{ij} \approx \frac{1}{T}\left\{\left[c_1 + c_2\frac{\mathrm{II}}{(2E)^2}\right]\Delta E_{ij} + c_3\frac{\Delta E_{ik}\Delta E_{kj} - \frac{1}{3}\mathrm{II}\delta_{ij}}{2E}\right\}, \tag{30}$$

$$\mathrm{II} = \Delta E_{ij}\Delta E_{ji}, \quad E = \tfrac{1}{2}E_{kk}.$$

We use $T = L_f/E^{\frac{1}{2}}$ and ΔE_{ij} is defined in (25). The value of c_3 was found to be dependent upon the sign of the anisotropy: c_3 is negative for runs *A*1, *A*2, *P*1, *P*2 and *U*1, which all start with $E_{33} < E_{11}$; it is positive for *U*2, where $E_{33} > E_{11}$. The last term in (30) is quadratic in ΔE_{ij} and does not change sign if the sign of ΔE_{ij} is changed, whereas $\operatorname{sgn}\Phi_{ij} = \operatorname{sgn}\Delta E_{ij}$ for the steady state. The factor c_3 does not seem to have a universal value. This might change if we expand the model such that the highest-order term is an odd function of ΔE_{ij}. Here we set $c_3 \equiv 0$. Using similar arguments, Reynolds (1974) came to the same conclusion. The values of c_1 and c_2, as found by a least-squares fit, are given in table 3 together with the r.m.s. error δ computed from (27), using Φ_{ij}^m as defined by (30). We get negative values of c_2, which means that the rate of return to isotropy decreases if the departure from isotropy becomes large. Using $E_{ij}^2 \leqslant E_{ii}E_{jj}$ for $j \neq i$ (without summation) it is easy to show that $\mathrm{II}/(2E)^2 \leqslant \frac{2}{3}$. This relationship holds for any anisotropic turbulence. In order to ensure a positive correlation between Φ_{ij} and ΔE_{ij} for *any* possible value of $\mathrm{II}/(2E)^2$, we therefore require

$$c_2 \geqslant -\tfrac{3}{2}c_1, \quad c_1 > 0. \tag{31}$$

For axisymmetric turbulence, we find $\mathrm{II}/(2E)^2 = \frac{2}{3}$ if $E_{11} = E_{22} = 0$, $E_{33} > 0$. In this case $\partial u_3/\partial x_3$ is also zero, so that all components of the pressure–strain correlation are zero. Therefore it might be appropriate to require $c_2 = -\frac{3}{2}c_1$. Table 3 shows that the empirical values of c_2 are even smaller than is required by (31). This is allowed if the departure from isotropy is so small that $c_1 + c_2\mathrm{II}/(2E)^2 > 0$. However, a generally acceptable model seems to be (30), with $c_1 = 1{\cdot}0$, $c_2 = -1{\cdot}5$ and $c_3 = 0$.

In spite of our analysis, it is still possible that the rate of return to isotropy might be relatively larger for small departures from isotropy. This is suggested by the experimental results of Tucker & Reynolds (1968).† We cannot exclude or confirm this possibility since the statistical errors become prohibitive for small departures from isotropy. Such changes in the value of Φ_{ij} for small and large values of II could be accounted for by adding a term proportional to $(\mathrm{II}/(2E)^2)^2\Delta E_{ij}/T$ to (30).

† This fact has been pointed out to us by one of the referees.

5.4. *Local wavenumber dependence of Rotta's constant*

In order to see the wavenumber dependence of Rotta's 'constant' we define a $\hat{c}(k)$ by

$$\hat{\Phi}_{ij} = -\hat{c}(k)\frac{\hat{\epsilon}}{\hat{E}}(\hat{E}_{ij} - \tfrac{1}{3}\delta_{ij}\hat{E}_{kk}). \tag{32}$$

Here all quantities are functions of k and t. Again we determine $\hat{c}(k)$ by a least-squares fit, requiring

$$\sum_t \sum_{i=1}^{3} \sum_{j=1}^{3} [\hat{\Phi}_{ij}(k,t) - \Phi^m_{ij}(k,t)]^2 = \text{minimum},$$

where $\Phi^m_{ij}(k,t)$ is the value predicted by (32). We sum over all time steps t where t is larger than $0{\cdot}2L_f/v$ in order to allow the formation of triple correlations. The resultant values of $\hat{c}(k)$ are plotted in figure 10. The peak cases $P1$ and $P2$ show that $\hat{c}(k)$ is small where the main anisotropy occurs but larger at some higher wavenumbers which reflect the shift in wavenumber space between $\Delta\hat{E}_{ij}$ and $\hat{\Phi}_{ij}$. A general decreasing tendency for increasing wavenumbers can be seen.

5.5. *Fine-scale motion and effects of strain*

Several authors (e.g. Rotta 1951; Reynolds 1976; Naot *et al.* 1970; Hanjalić & Launder 1972; Rodi 1972; Shir 1973) have proposed extending the models for the pressure–strain correlation by terms accounting for strain and for the resulting anisotropy in the different production terms contributing to the time variation of E_{ij}. In the present runs the mean production terms are zero. However, if we split our flow field into two parts, one containing the large-scale motion defined by $|\mathbf{k}| \leqslant k_0$ and the other the fine-scale motion ($|\mathbf{k}| > k_0$), where k_0 is some arbitrary positive wavenumber, we may investigate the pressure–strain correlation for the fine-scale motion where the production terms are no longer zero.

We define fine-scale quantities $y'(k)$ by

$$y'(k_0) = \sum_{k=k_0}^{k_1} y(k) \quad (k_1 = (242)^{\frac{1}{2}}k_{\min}), \tag{33}$$

where y stands for Φ_{ij}, E_{ij}, Γ_{ij}, etc. The integral length scale $Lf(k_0)$ of the fine-scale motion is

$$L'_f(k_0) = \frac{3\pi}{4E'(k_0)} \sum_{k=k_0}^{k_1} \frac{1}{k}\hat{E}(k). \tag{34}$$

If we use Rotta's model (24), we find that the appropriate value of c' increases strongly with growing k_0 and the errors δ' become large. In order to get a value of c' independent of k_0 and to reduce the errors we should account for the anisotropic production Γ'_{ij}. We use the proposal of Naot *et al.* (1970) and Rodi (1972):

$$\phi'_{ij} = c_3\frac{E'^{\frac{1}{2}}}{L'_f}\Delta E'_{ij} - c_4(\Gamma'_{ij} - \tfrac{1}{3}\delta_{ij}\Gamma'_{kk}), \tag{35}$$

where all quantities are functions of k_0 and t. By a least-squares fit we determine $c_3(k_0)$ and $c_4(k_0)$. The results for run $A2$ (the run with the smallest statistical errors) are given in table 4. Here, again, δ is the r.m.s. error. The results for very small wavenumbers are not listed in this table as Γ'_{ij} is small here and the results for c_4 would

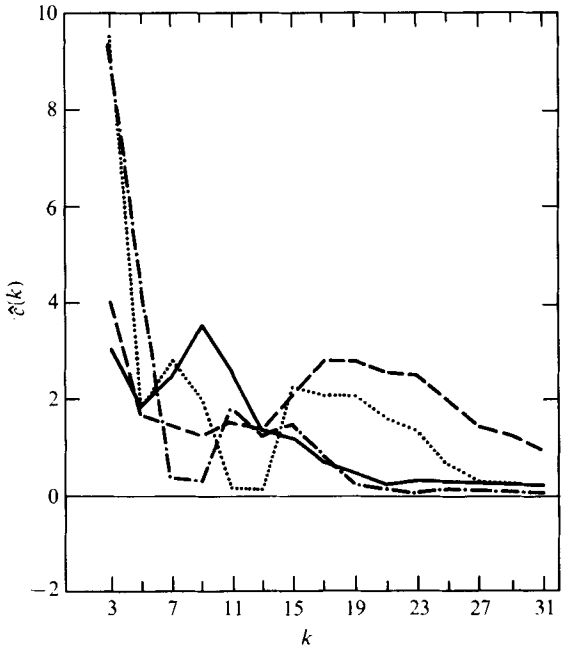

FIGURE 10. Local Rotta constant $\hat{c}(k)$ *vs.* wavenumber k for different runs. ——, $A1$; — —, $A2$; —·—, $P1$; ·····, $P2$.

k_0	c_1	c_2	δ
8	0·939	0·824	0·072
10	1·174	0·596	0·079
12	1·735	0·372	0·066
14	−0·736	1·16	0·065
16	0·042	0·785	0·054
18	0·721	0·603	0·077
20	1·16	0·524	0·095
22	1·61	0·468	0·109
24	2·07	0·406	0·125
26	2·35	0·377	0·149
28	1·94	0·416	0·172
30	0·35	0·468	0·216

TABLE 4. Effects of anisotropic energy production (see § 5.5).

therefore not be significant. The value $c_3(k_0)$ is identical to c' in the limit $k_0 = 0$. We find that for small wavenumbers k_0 the pressure–strain correlation is controlled by $\Delta E'_{ij}$. For large wavenumbers, however, the production terms Γ'_{ij} become dominant. Although the scatter in c_3 and c_4 is large owing to statistical fluctuations, we see that both are nearly independent of k_0. Typical values are $c_3 \approx 0{\cdot}7$ (which corresponds to c') and $c_4 \approx 0{\cdot}6$. Naot *et al.* (1970) used $c_3 \equiv 0$ and deduced c_4 to be between 0·66 and 0·8 from different experiments; Rodi (1972) used a value $c_4 = 0{\cdot}5$. These values agree surprisingly well with the numerical results.

6. Summary

We have used the spectral method of Orszag & Patterson (1972*a*, *b*) as extended in I for the direct numerical simulation of pressure and velocity fluctuations in three-dimensional space. In this paper we considered axisymmetric homogeneous decaying turbulence with $Re_\lambda \lesssim 40$ (except for runs $U1$ and $U2$, where $Re_\lambda = \infty$). We described several runs with different axisymmetric (highly anisotropic) Gaussian initial conditions. The numerical results are summarized in table 5. The main limitations of the present runs are statistical fluctuations in the mean values obtained for one realization. They can be reduced by averaging over ensembles of realizations as we did for two cases. The statistical uncertainties for the value of Rotta's constant are of the order of 20 % for the present single realizations. They would be much larger if we considered small initial anisotropies because then the departure of isotropy would become small compared with the statistical fluctuations.

Spectral as well as mean values of the different correlations governing the time evolution of the tensorial energy components are shown. As expected, we found that the pressure–strain correlation causes the return to isotropy. The return to isotropy is, however, not determined kinematically; rather, it depends upon triple correlations that are created by the flow dynamics. Although these triple correlations are independent of the skewness S, both vary on about the same characteristic time scales.

With respect to the spectral distribution of the pressure–strain correlation, we found that at some wavenumbers this correlation is the result of the anisotropy at a wavenumber that is smaller by a factor of $0{\cdot}7 \pm 0{\cdot}2$. The spectral distribution is, moreover, much broader than the kinetic energy distribution; the same is true for the pressure spectrum. The rate of return to isotropy is larger at high wavenumbers than at low wavenumbers.

The inertial energy transfer rate has been found to be anisotropic and proportional to the anisotropy of the energy tensor. This transfer rate tends to produce anisotropy at high wavenumbers, therefore. Whether we get an overrelaxation to an anisotropic state of opposite sign depends upon the relative magnitude of the pressure and inertial transfer. If the latter is smaller than the former, no overrelaxation occurs.

Rotta's model is appropriate if the characteristic time scale of the total flow is larger than $0{\cdot}2\,L_f/v$, which is the time scale for the triple correlations. Moreover, the departure from isotropy must be small enough since Rotta's model does not account for the kinematical constraint, $\Phi_{ij} = 0$ if $\partial u_i/\partial x_j + \partial u_j/\partial x_i = 0$. Moreover, the length scales L_{ij} should not depart from the isotropic state more than does E_{ij}. Finally, we confirmed Herring's (1974) result in that the constant c' in (24) is less dependent than c in (23) upon the initial conditions. The resultant value of Rotta's constant is $c' \simeq 0{\cdot}8$, which is about 20 % less than the value found by Herring (1974). However, this is not a large difference in view of the simplifying assumptions used by Herring (see also Schumann & Herring 1976). If we use the relation between the dissipation and $E^{\frac{3}{2}}/L_f$ (as given in I), (24) can be incorporated into semi-empirical turbulence models. For large Reynolds numbers (23) is appropriate with $c = c'/B_2$ ($B_2 \simeq 0{\cdot}7$ according to I), resulting in $c \simeq 1{\cdot}1$.

No conclusive result was obtained for the influence of anisotropies in the length scales. With respect to the proposal of Lumley & Khajeh-Nouri (1974), we suggested dropping the highest-order term; we also found a relationship that should be obeyed

	Time	*A1*	*A2*	*P1*	*P2*	*L1*	*L2*	*U1*	*U2*
$\frac{1}{2}(E_{11}+E_{22})$	0	1·545	1·485	1·015	1·037	1·062	1·334	1·525	0·830
	0·2	1·265	0·884	0·565	0·273	0·859	1·176	1·158	1·562
	0·4	0·976	0·763	0·295	0·080	0·638	0·989	1·061	1·745
	0·8	0·567	0·210	—	—	—	—	—	—
E_{33}	0	0	0	0	0	1·250	0·996	0	3·343
	0·2	0·168	0·246	0·076	0·060	1·024	0·931	0·759	1·946
	0·4	0·312	0·236	0·078	0·028	0·755	0·825	0·964	1·805
	0·8	0·353	0·129	—	—	—	—	—	—
Φ_{33}	0	0	0	0	0	−0·656	−0·112	0	0·139
	0·2	1·272	1·395	0·553	0·320	−0·185	0·536	2·093	−2·737
	0·4	0·858	0·444	0·187	0·036	−0·333	0·193	0·438	0·064
	0·8	0·379	0·071	—	—	—	—	—	—
$\frac{1}{2}(\epsilon_{11}+\epsilon_{22})$	0	0·958	2·479	2·462	5·857	1·118	0·582	0	0
	0·2	0·912	1·878	1·564	1·710	1·291	0·683	0	0
	0·4	0·890	1·103	0·827	0·406	1·140	0·820	0	0
	0·8	0·576	0·342	—	—	—	—	—	—
ϵ_{33}	0	0	0	0	0	0·786	0·674	0	0
	0·2	0·238	0·906	0·340	0·478	1·020	0·792	0	0
	0·4	0·444	0·740	0·288	0·144	1·004	0·932	0	0
	0·8	0·446	0·264	—	—	—	—	—	—
L_f	0	0·592	0·271	0·592	0·201	0·438	0·587	0·111	0·111
	0·2	0·554	0·276	0·314	0·208	0·421	0·574	0·112	0·112
	0·4	0·538	0·292	0·331	0·250	0·420	0·552	0·113	0·113
	0·8	0·537	0·345	—	—	—	—	—	—

TABLE 5. Numerical results for the tensorial energies E_{ij}, the pressure–strain correlations Φ_{ij}, the dissipation ϵ_i, and the integral length scale L_f. Note that all tensor components are zero for $i \neq j$ and that the 11 components are equal to the 22 components; also $\Phi_{11} = \Phi_{22} = -\frac{1}{2}\Phi_{22}$.

by the two remaining constants; some values for these constants have been proposed. By splitting the flow into large- and fine-scale motions we were able to obtain information about the influence of anisotropic production terms; the results agree well with the predictions of Naot *et al.* (1970) and Rodi (1972).

The authors thank Dr J. R. Herring for stimulating discussions and encouragement. He proposed the algorithm for generating the initial values. After completion of the present study we learned of a similar investigation by Dr Steven A. Orszag (private communication, unpublished.) This work was done while U. Schumann was with the Advanced Study Program at the National Center for Atmospheric Research, which is sponsored by the National Science Foundation.

Appendix. Generation of random axisymmetrically isotropic velocity fields

We choose $a_1(\mathbf{k})$, $a_2(\mathbf{k})$, $b_1(\mathbf{k})$ and $b_2(\mathbf{k})$ to be zero-mean Gaussian, independent, real, random, scalar fields such that

$$A(\mathbf{k}) = a_1(\mathbf{k}) + ia_2(\mathbf{k}), \quad B(\mathbf{k}) = b_1(\mathbf{k}) + ib_2(\mathbf{k})$$

have the properties $A(\mathbf{k}) = A^*(-\mathbf{k}), \quad B(\mathbf{k}) = B^*(-\mathbf{k}),$

$$\langle A(\mathbf{k}) B(-\mathbf{k})\rangle = 0,$$

$$\langle A(\mathbf{k}) A(-\mathbf{k}')\rangle = \langle B(\mathbf{k}) B(-\mathbf{k}')\rangle = 0 \quad \text{if} \quad \mathbf{k} \neq \mathbf{k}',$$

$$\langle A(\mathbf{k}) A(-\mathbf{k})\rangle = \Phi^1(\mathbf{k}), \quad \langle B(\mathbf{k}) B(-\mathbf{k})\rangle = \Phi^2(\mathbf{k}).$$

Then
$$\hat{\mathbf{u}}(\mathbf{k}) = A(\mathbf{k})\,\mathbf{e}^1(\mathbf{k}) + B(\mathbf{k})\,\mathbf{e}^2(\mathbf{k}), \tag{A 1}$$

where $\mathbf{e}^1$ and $\mathbf{e}^2$ are defined by (2), is a Gaussian velocity field with zero mean and

$$\langle \hat{u}_i(\mathbf{k})\,\hat{u}_j(-\mathbf{k}')\rangle = \begin{cases} 0 & \text{if} \quad \mathbf{k} \neq \mathbf{k}', \\ \sum_{\alpha=1}^{2} \Phi^\alpha(\mathbf{k})\, e_i^\alpha(\mathbf{k})\, e_j^\alpha(\mathbf{k}) & \text{if} \quad \mathbf{k} = \mathbf{k}', \end{cases}$$

$$k_i\,\hat{u}_i(\mathbf{k}) = 0.$$

The components of the energy tensor $\hat{E}_{ij}(k)$ are

$$\hat{E}_{ij}(|\mathbf{k}|) = k^2 \int_{\theta=0}^{\pi} \int_{\phi=0}^{2\pi} \langle \hat{u}_i(\mathbf{k})\,\hat{u}_j(-\mathbf{k})\rangle \sin\theta\, d\theta\, d\phi,$$

where
$$\mathbf{k} = \{\sin\theta\cos\phi, \sin\theta\sin\phi, \cos\theta\}.$$

The resultant non-zero components are

$$\hat{E}_{11}(k) = \hat{E}_{22}(k) = 4\pi k^2[\tfrac{1}{2}\Phi_0^1(k) + \tfrac{1}{6}\Phi_0^2(k) + \tfrac{1}{15}\Phi_2^2(k)], \tag{A 2}$$

$$\hat{E}_{33}(k) = 4\pi k^2[\tfrac{2}{3}\Phi_0^2(k) - \tfrac{2}{15}\Phi_2^2(k)],$$

where we describe the angular dependence of $\Phi^\alpha(\mathbf{k})$ by the Legendre moments (Herring 1974)

$$\Phi_l^\alpha(k) = \frac{2l+1}{2} \int_{-1}^{1} P_l(\mu)\, \Phi^\alpha(\mu)\, d\mu, \quad l = 0, 2, \quad \alpha = 1, 2,$$

$$\mu = (\mathbf{n}\cdot\mathbf{k})/k, \quad P_0(\mu) = 1, \quad P_2(\mu) = \tfrac{1}{2}(3\mu^2 - 1).$$

REFERENCES

Batchelor, G. K. 1946 The theory of axisymmetric turbulence. *Proc. Roy. Soc.* A **186**, 480–502.

Batchelor, G. K. 1959 *The Theory of Homogeneous Turbulence*. Cambridge University Press.

Champagne, F. H., Harris, V. G. & Corrsin, S. 1970 Experiments on nearly homogeneous turbulent shear flow. *J. Fluid Mech.* **41**, 81–139.

Daly, B. J. 1974 A numerical study of turbulence transitions in convective flow. *J. Fluid Mech.* **64**, 129–165.

DEARDORFF, J. W. 1974 Three-dimensional numerical study of turbulence in an entraining mixed layer. *Boundary-Layer Met.* **7**, 199–226.

DONALDSON, C. DUP. 1972 Calculation of turbulent shear flows for atmospheric and vortex motions. *A.I.A.A. J.* **10**, 4–12.

ELLIOT, J. A. 1972 Microscale pressure fluctuations measured within the lower atmospheric boundary layer. *J. Fluid Mech.* **53**, 351–383.

HANJALIĆ, K. & LAUNDER, B. E. 1972 A Reynolds stress model of turbulence and its application to thin shear flows. *J. Fluid Mech.* **52**, 609–638.

HERRING, J. R. 1974 Approach of axisymmetric turbulence to isotropy. *Phys. Fluids* **17**, 859–872 (and corrigendum *Phys. Fluids*, **19** (1976), 177).

KRAICHNAN, R. H. 1956 Pressure field within homogeneous anisotropic turbulence. *J. Acoust. Soc. Am.* **28**, 64–72.

LEE, T. D. 1952 On some statistical properties of hydrodynamical and magneto-hydrodynamical fields. *J. Appl. Math.* **10**, 69–74.

LUMLEY, J. L. & KHAJEH-NOURI, B. 1974 Computational modelling of turbulent transport. *Adv. Geophys.* A **18**, 169–192.

NAOT, D., SHAVIT, A. & WOLFSHTEIN, M. 1970 Interactions between components of the turbulent velocity correlation tensor due to pressure fluctuations. *Israel J. Tech.* **8**, 259–269.

ORSZAG, S. A. 1969 Numerical methods for the simulation of turbulence. *Phys. Fluids Suppl.* **12**, II 250–257.

ORSZAG, S. A. & PATTERSON, G. S. 1972*a* Numerical simulation of turbulence. In *Statistical Models and Turbulence*, pp. 127–147. Springer.

ORSZAG, S. A. & PATTERSON, G. S. 1972*b* Numerical simulation of three-dimensional homogeneous isotropic turbulence. *Phys. Rev. Lett.* **28**, 76–79.

REYNOLDS, W. C. 1974 Computation of turbulent flows. *A.I.A.A. Paper* no. 74–556.

REYNOLDS, W. C. 1976 Computation of turbulent flows. *Ann. Rev. Fluid Mech.* **8**, 183–208.

RODI, W. 1972 The prediction of free turbulent boundary layers by use of a two-equation model of turbulence. Ph.D. thesis, Mech. Engng Dept., Imperial College, London.

ROTTA, J. 1951 Statistische Theorie nichthomogener Turbulenz. *Z. Phys.* **129**, 547–572.

SCHUMANN, U. 1975 Numerical results for the pressure–strain correlation in channel flows. *Rep.* KFK-Ext 8/75-7.

SCHUMANN, U. 1976 Numerical simulation of the transition from three- to two-dimensional turbulence under a uniform magnetic field. *J. Fluid Mech.* **74**, 31–58.

SCHUMANN, U. & HERRING, J. R. 1976 Axisymmetric homogeneous turbulence: a comparison of direct spectral simulations with the direct-interaction approximation. *J. Fluid Mech.* **76**, 755–782.

SCHUMANN, U. & PATTERSON, G. S. 1978 Numerical study of pressure and velocity fluctuations in nearly isotropic turbulence. *J. Fluid Mech.* **88**, 685–709.

SHIR, C. C. 1973 A preliminary numerical study of atmospheric turbulent flows in the idealized planetary boundary layer. *J. Atmos. Sci.* **30**, 1327–1339.

TUCKER, H. J. & REYNOLDS, A. J. 1968 The distortion of turbulence by irrotational plane strain. *J. Fluid Mech.* **32**, 657–673.

UBEROI, M. S. 1953 Quadruple velocity correlations and pressure fluctuations in isotropic turbulence. *J. Aero. Sci.* **20**, 197–204.